Cryoscope

A technology pathfinder for time domain astronomy in the NIR

Roger Smith and Mansi Kasliwal

The convergence of many new technologies will soon enable high cadence surveys of the infrared sky for the first time. We describe a pathfinder telescope currently under construction, which will demonstrate a technology for imaging over a field of view two orders of magnitude greater than previously achieved in the thermal infrared. The novel optical design not only delivers diffraction limited image quality over large fields, but its double meniscus corrector serves as the entrance window to a fully cryogenic optical path that assures low thermal background in spite of the large field of view. We describe the window manufacturing and support strategies which allow scaling to apertures larger than a meter, and the various methods to prevent ice precipitation. A new, cheaper, growth process for large format infrared detectors is showing promise of making a 600 megapixel NIR focal plane feasible. High speed direct drive telescope mounts, now commercially available, will be upgraded to provide the vibration isolation necessary to take advantage of the exquisite seeing.

To catch transients in NIR

49 deg^2 every1000s with SNR>5 for magnitude 23.3 at $2.3<\lambda<2.55\mu m$

WIDE

- FoV = 0.6 deg^2

  = Current record

  VISTA @ ESO

DEEP

DARK

(Low sky background)

200 times wider field

WIDE

- **FoV = 47 deg^2**
- 24K * 24K pixels

Cheaper IR detectors developed by NSF-ATI

DEEP

DARK

Smaller pixels & darker sky

WIDE

- FoV = 47 deg^2
- 24K * 24K pixels

DEEP

- 1.2 m aperture
- 1 arcsec pixel
- Diffraction limited

DARK

- Dark sky @ 2.4μm
- Cold window (slightly above ambient)

30m tower

Dome C

Optics to match good seeing

Scan whole night sky in less than a “day”…

WIDE

- 47 deg^2 FoV
- 24K * 24K pixels

DEEP

- 1.2 m aperture
- 1 arcsec pixel
- **Diffraction limited**

Image stabilizing telescope mount

DARK

- Dark sky @ 2.4μm
- Cold window (slightly above ambient)
- **Cryogenic optical path**

New Optical design

Cheaper large format IR detectors: ✔ good QE

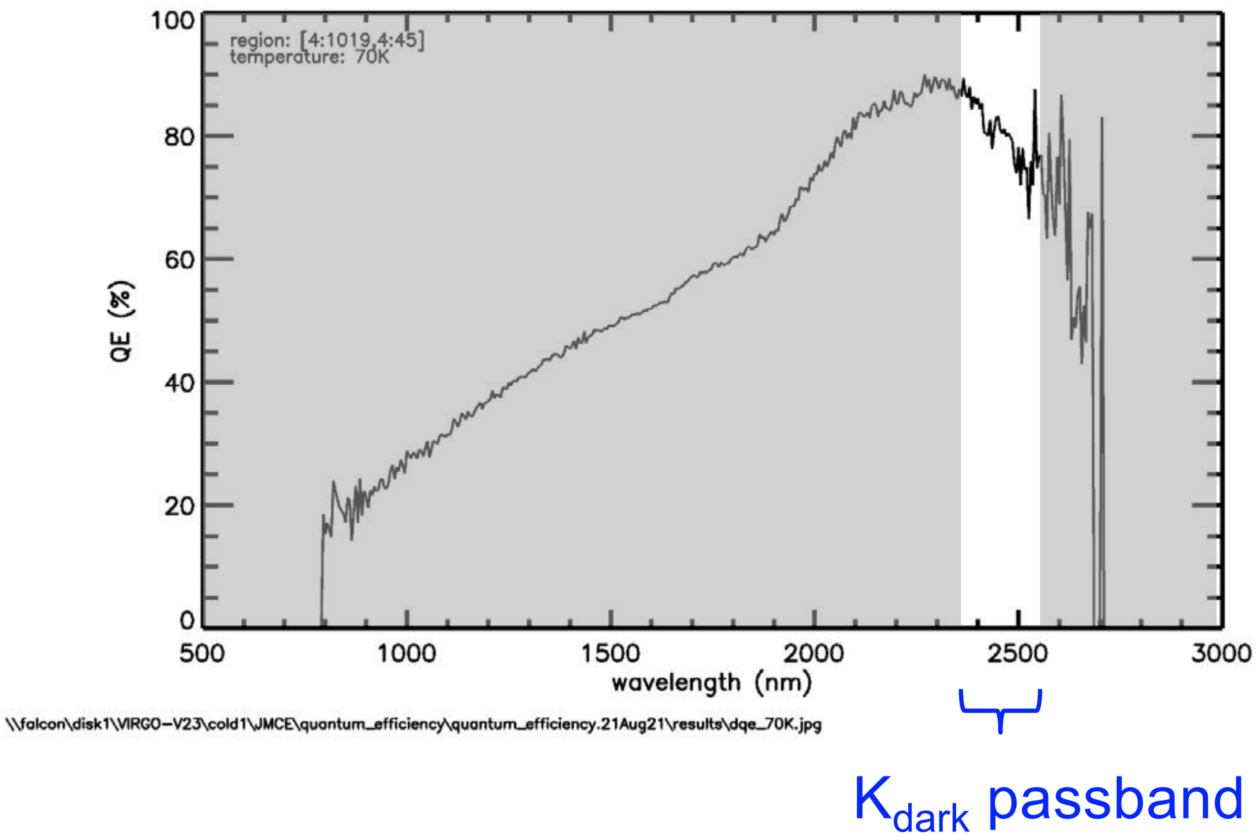

- NSF-ATI grant has funded development at Raytheon of MBE-on-silicon process for making large NIR detectors 4x cheaper. (PI: Don Figer)
- ~80% QE in K_dark passband
- Peak of QE curve can be tuned for peak in middle of passband.
- 27e- read noise prior to multiple sampling.

Low dark current. Tight noise distribution

- ✔ Require < 10 e−/s

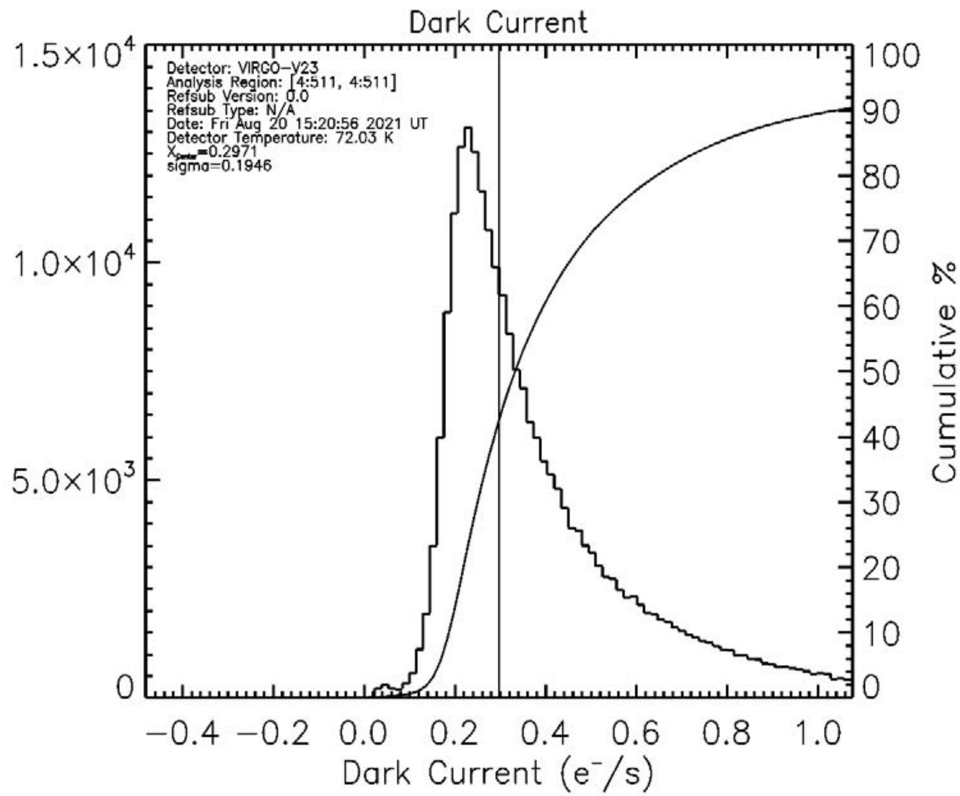

\\falcon\disk1\VIRGO−V23\cold1\JMCE\darkcurrent\darkcurrent.20Aug21_1\results\q4\noref\slopeplots\region2\histograms\dark_70K_893.127_utr_50_

- ✔ Require < 31 e-

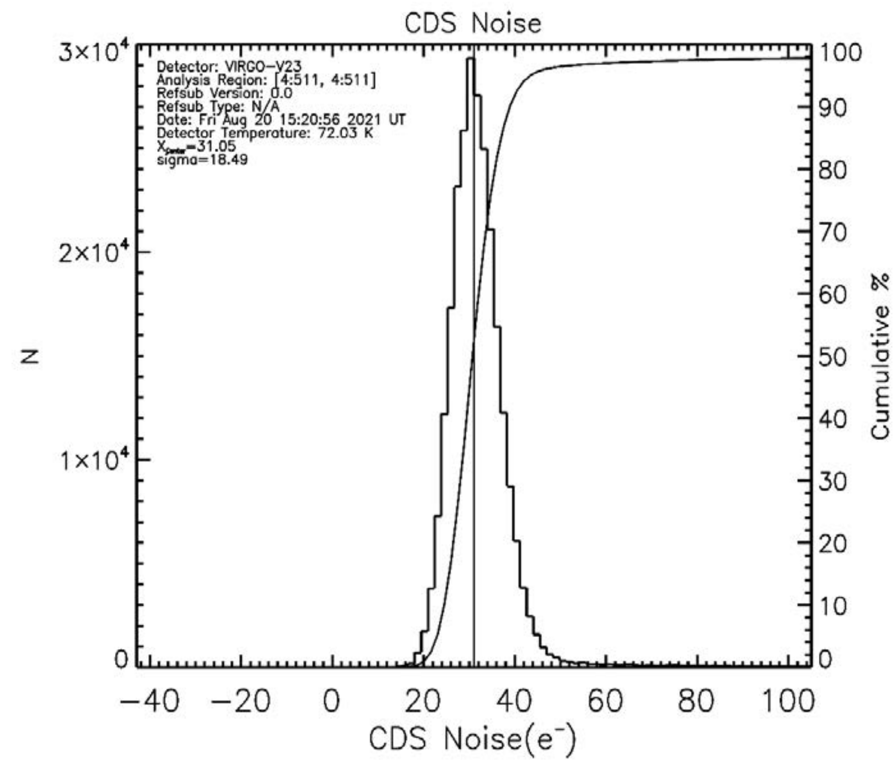

\\falcon\disk1\VIRGO−V23\cold1\JMCE\darkcurrent\darkcurrent.20Aug21_1\results\q4\noref\readnoise_results\region2\histograms\dark_70K

Hybridize to SC 4Kx6K ROIC

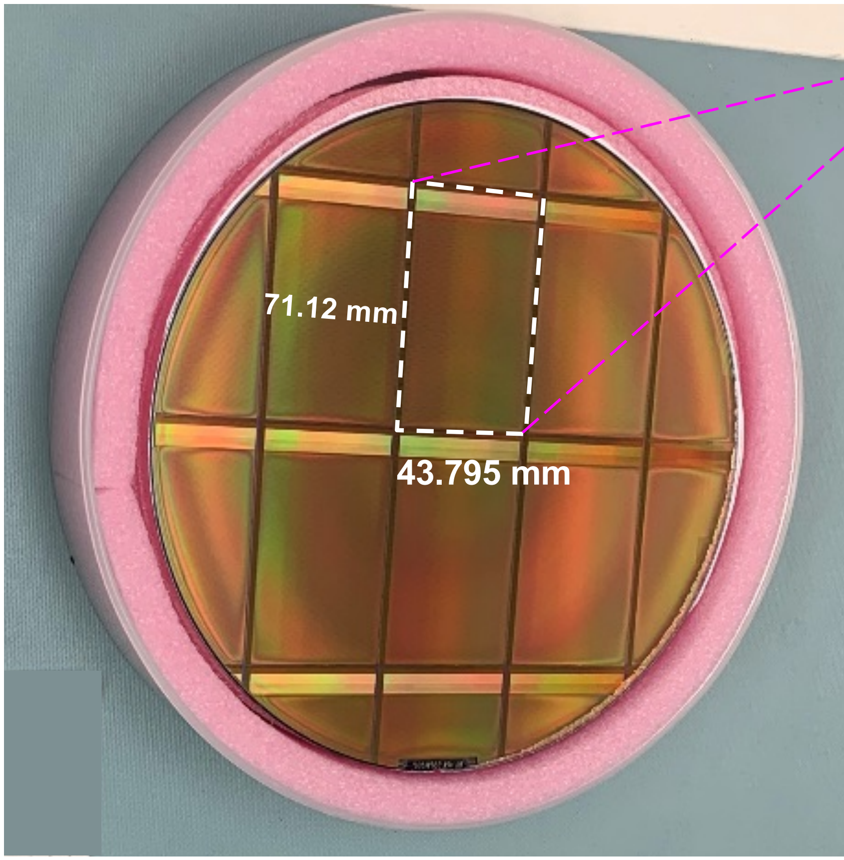

8" wafer

- 4K*6K Readout IC by Sensor Creations Inc
  - Funded by NASA SBIR grant (via WFIRST)
  - Currently under test
- Cryoscope will deploy 6x4 mosaic
  - 24K*24K pixels
  - Instantaneous Field of View = 49 deg^2
  - Beam obstruction by 6x4 mosaic is only 8%
- 10 μm pixels → 1.031 arcsec/pixel
  - telescope focal length = 2.0 m
  - 1.2m aperture
  - f/1.66

  → FWHM at diffraction limit = 4.2 μm

Air glow lines

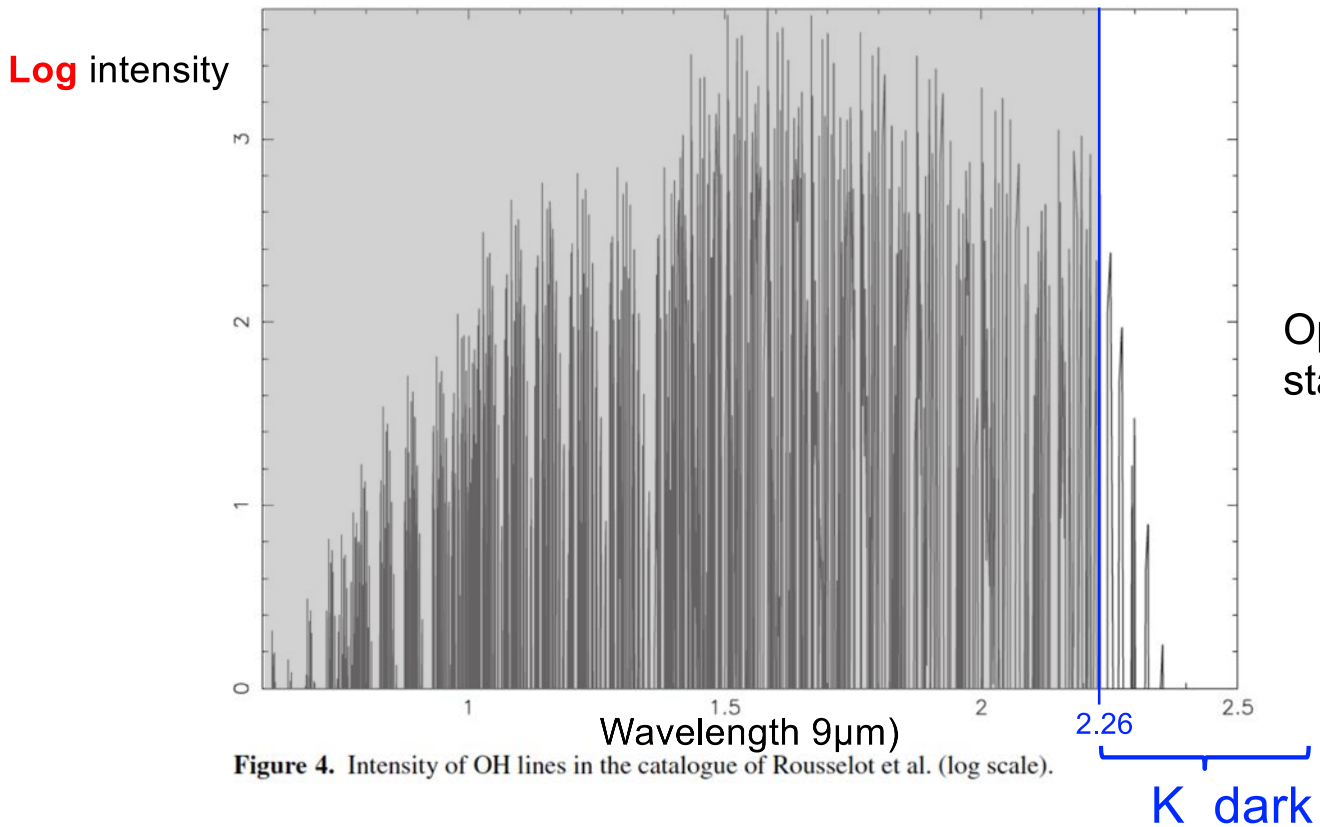

Figure 4. Intensity of OH lines in the catalogue of Rousselot et al. (log scale).

Optimum passband starts at 2.26 µm

South Pole - atmospheric transmission

Lower water column at Dome C
(higher altitude, lower temperature)

South Pole: 2835 m
Dome C: 3233 m
Dome A: 4093 m

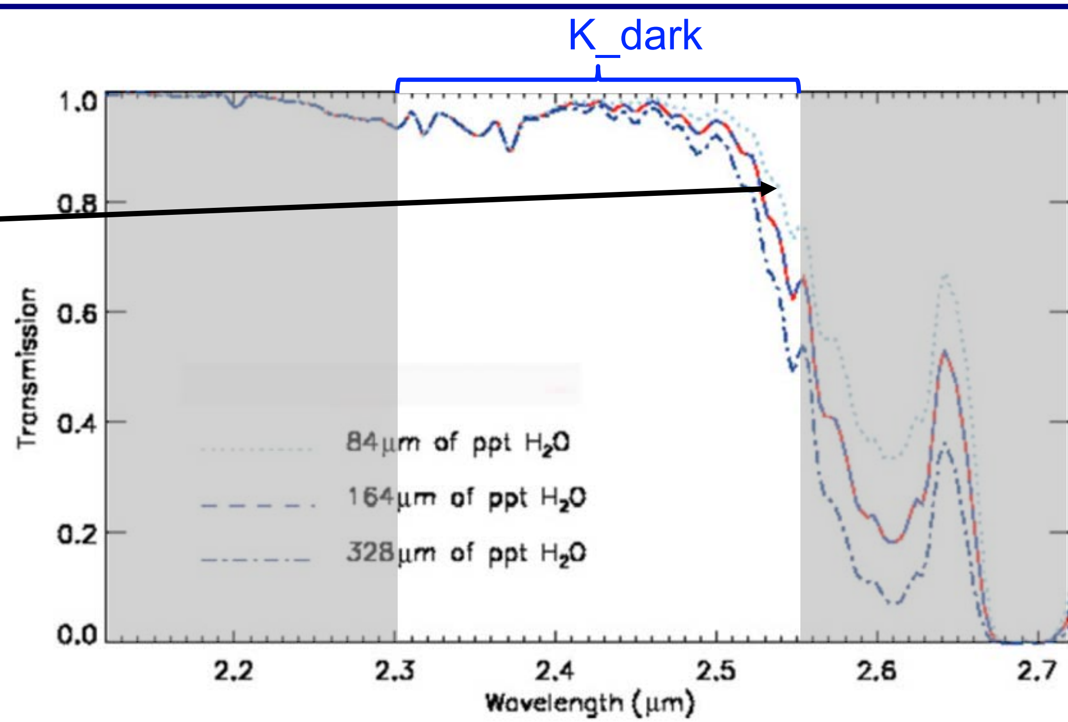

Figure 3. Curves of South Pole atmospheric transmission taken from Hidas et al. (2000), with varying assumptions about the atmospheric water content. The three lines are for precipitable water columns of 84, 164, and 328 μm.

Black body power density

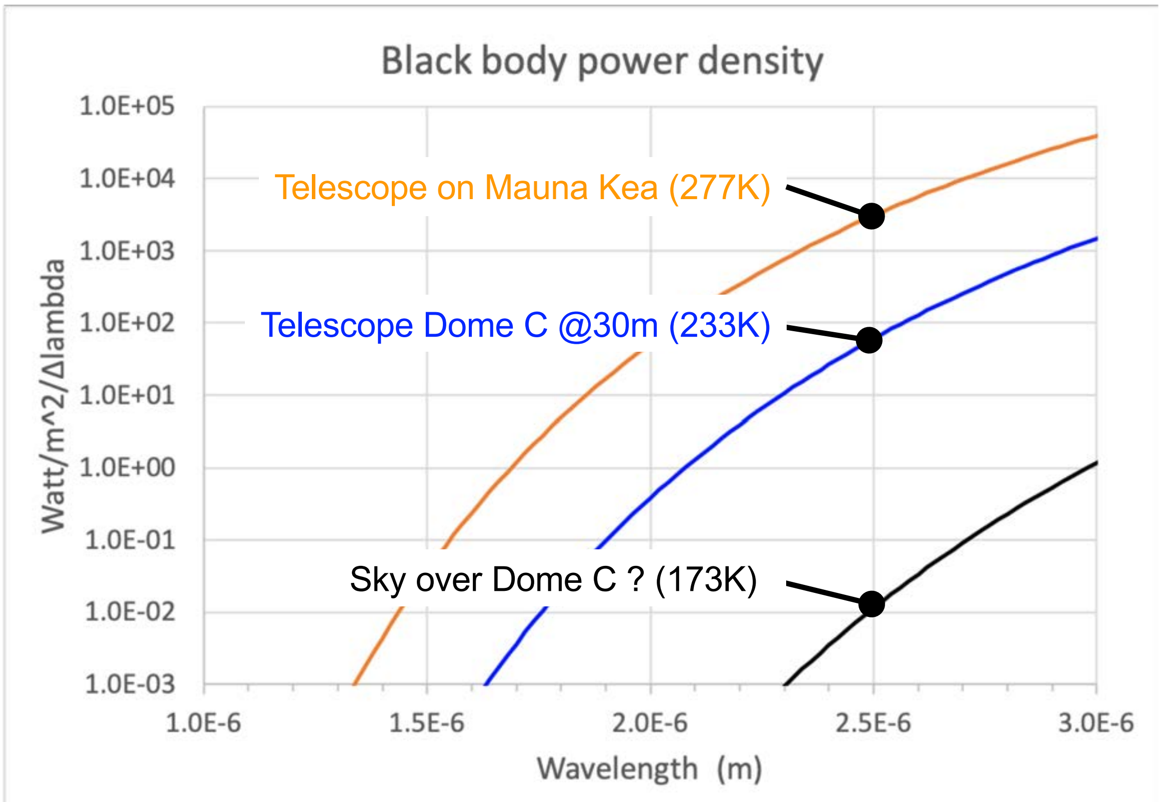

Reduced emission from telescope helps but very widefield designs have higher emissivity thus need to be as cold as sky.

Fucik Telescope

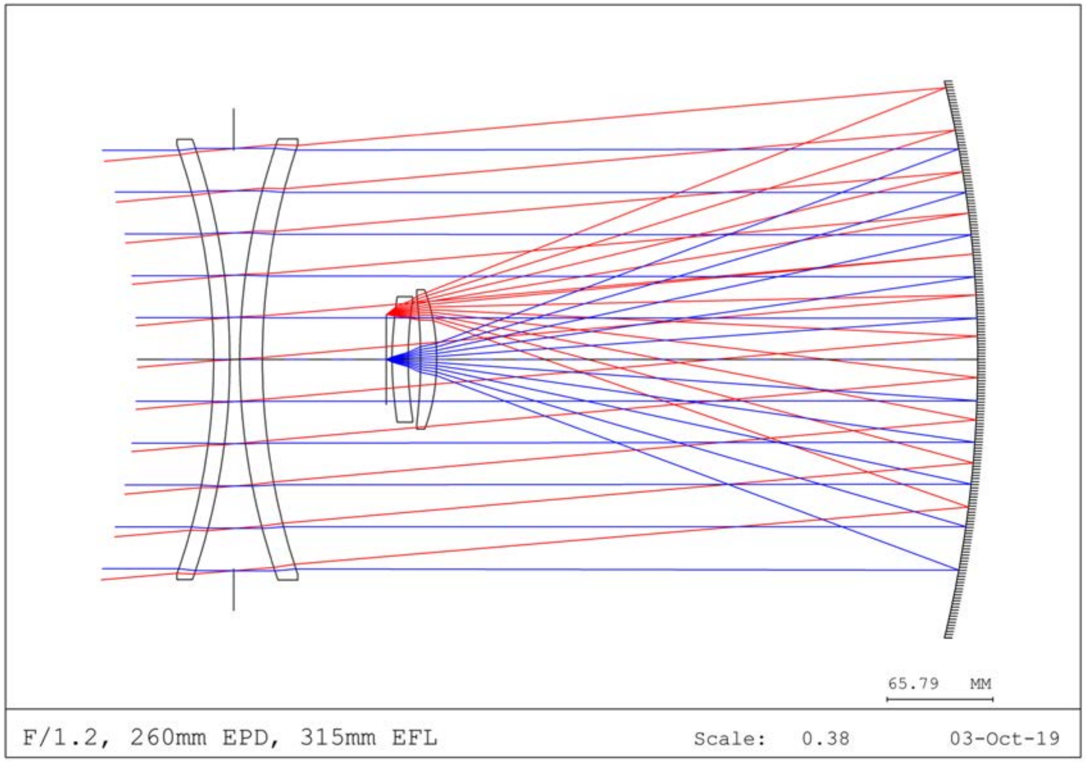

- Diffraction limited
  - ➢ Excellent image quality even at f1.2 and 100 sq.deg.
- All fused silica corrector → scalable to large aperture.
- Arizona Mirror labs are developing glass slumping to fabricate large menisci economically.
  - ➢ Similar lenses are used in prime focus correctors.
- Shorter than a Schmidt → smaller primary for given aperture and FoV

Negligible aberrations !

Pathfinder

- 4.06 deg x 4.06 deg field of view
- 260mm aperture at f/2

Spots are much smaller than 18 µm pixel

RMS radius < 1.2 µm

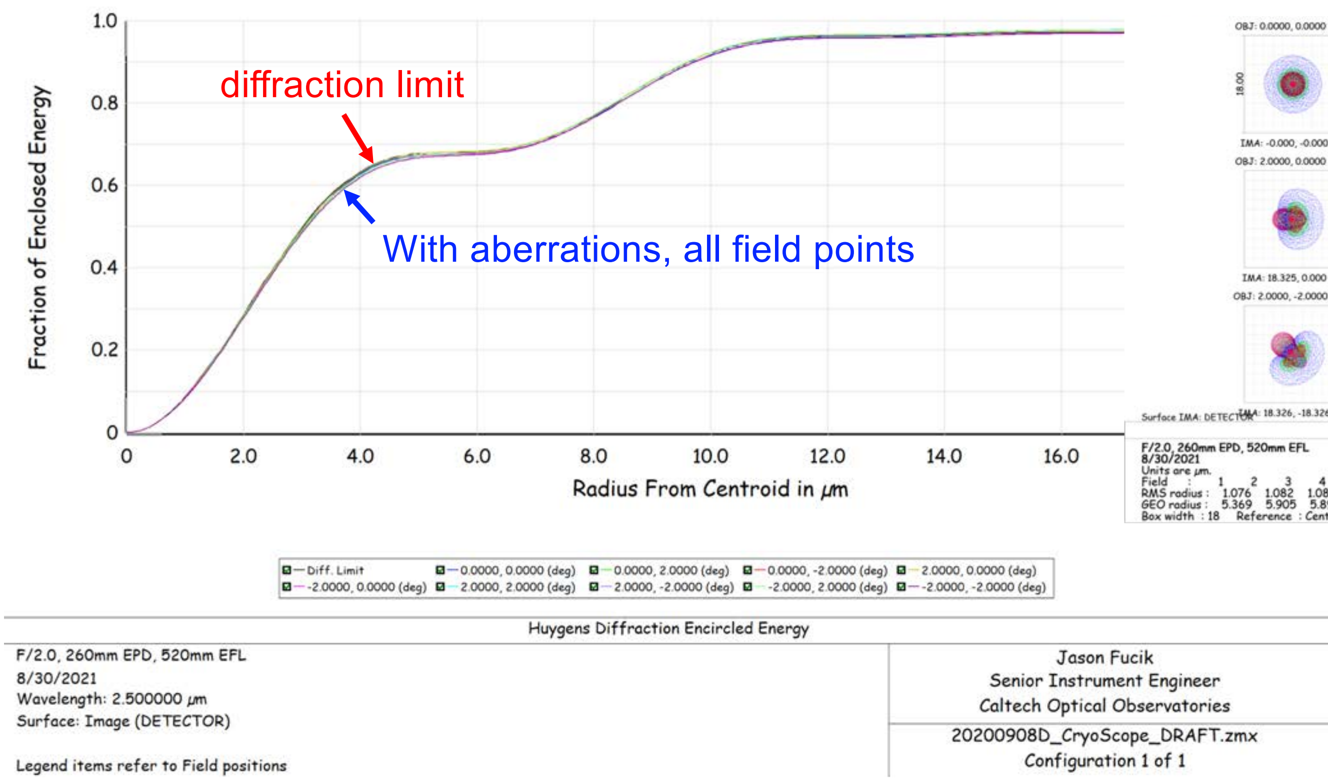

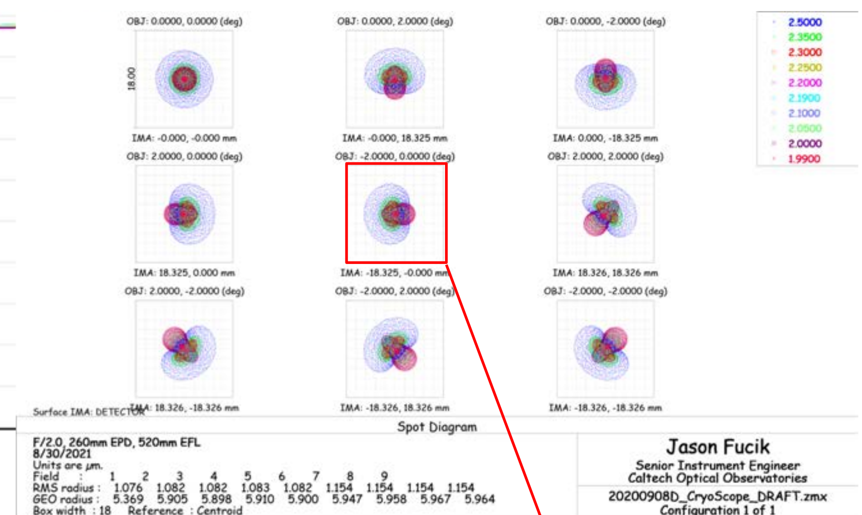

18µm pixel for pathfinder

Temperature profiles

PNRA radiosonde data

Dome C

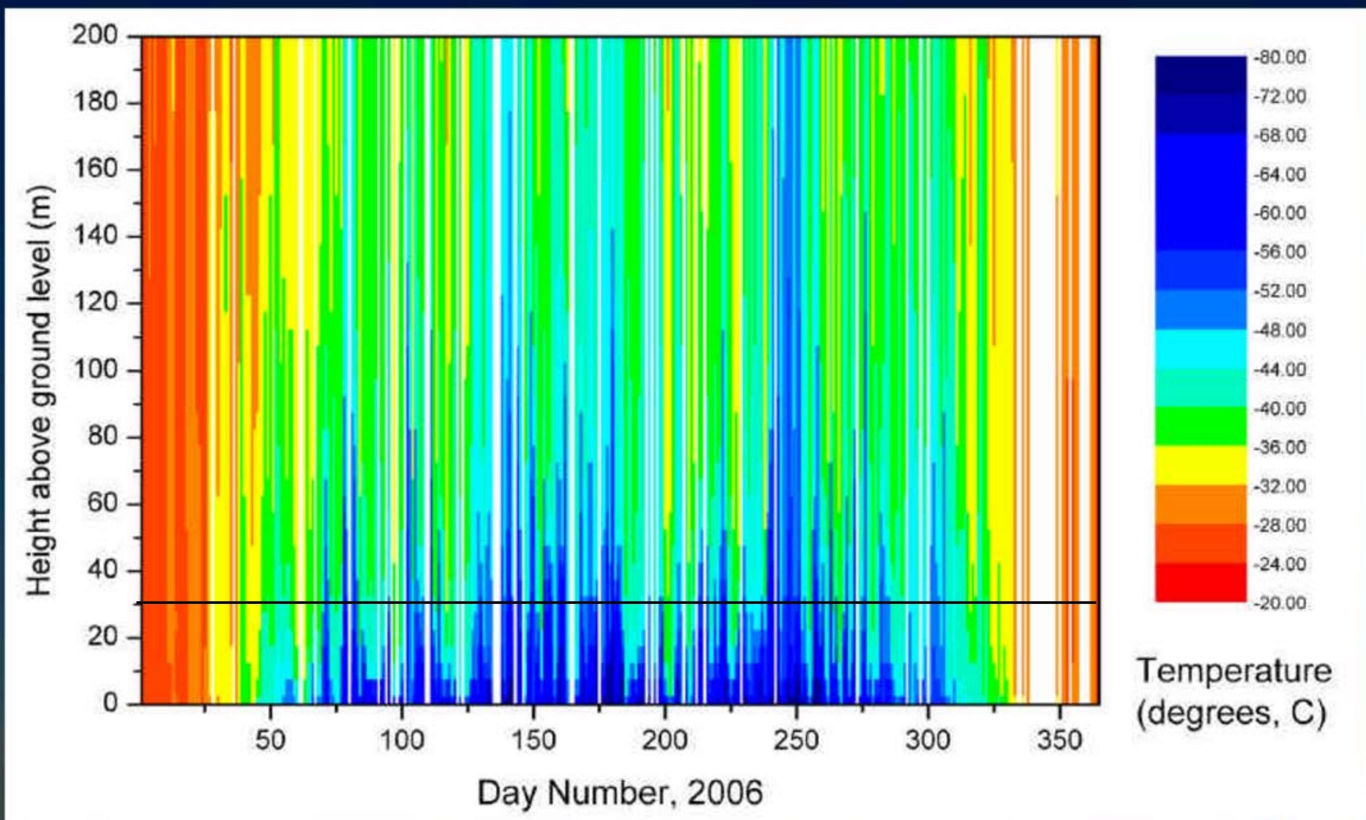

Will Saunders (AAO), Andrew McGrath (AAO), David Ward (AAO), Peter Gillingham (AAO), Jon Lawrence (UNSW), John Storey (UNSW)

Why a cryogenic telescope ?

Usual measures to block rays from warm telescope limit FoV.

…but without re-imaging optics and cold Lyot stop, telescope emissivity is closer to 1 than the ~2% emissivity of optics.

- At top of inversion layer (25-30m above ice), T= ~230 K ← not cold enough
- We really want telescope temperature < sky temperature < 200 K.
- 2nd corrector element of Fucik optical design can serve as window, so *full optical path can be cryogenically cooled.*

Cryoscope pathfinder

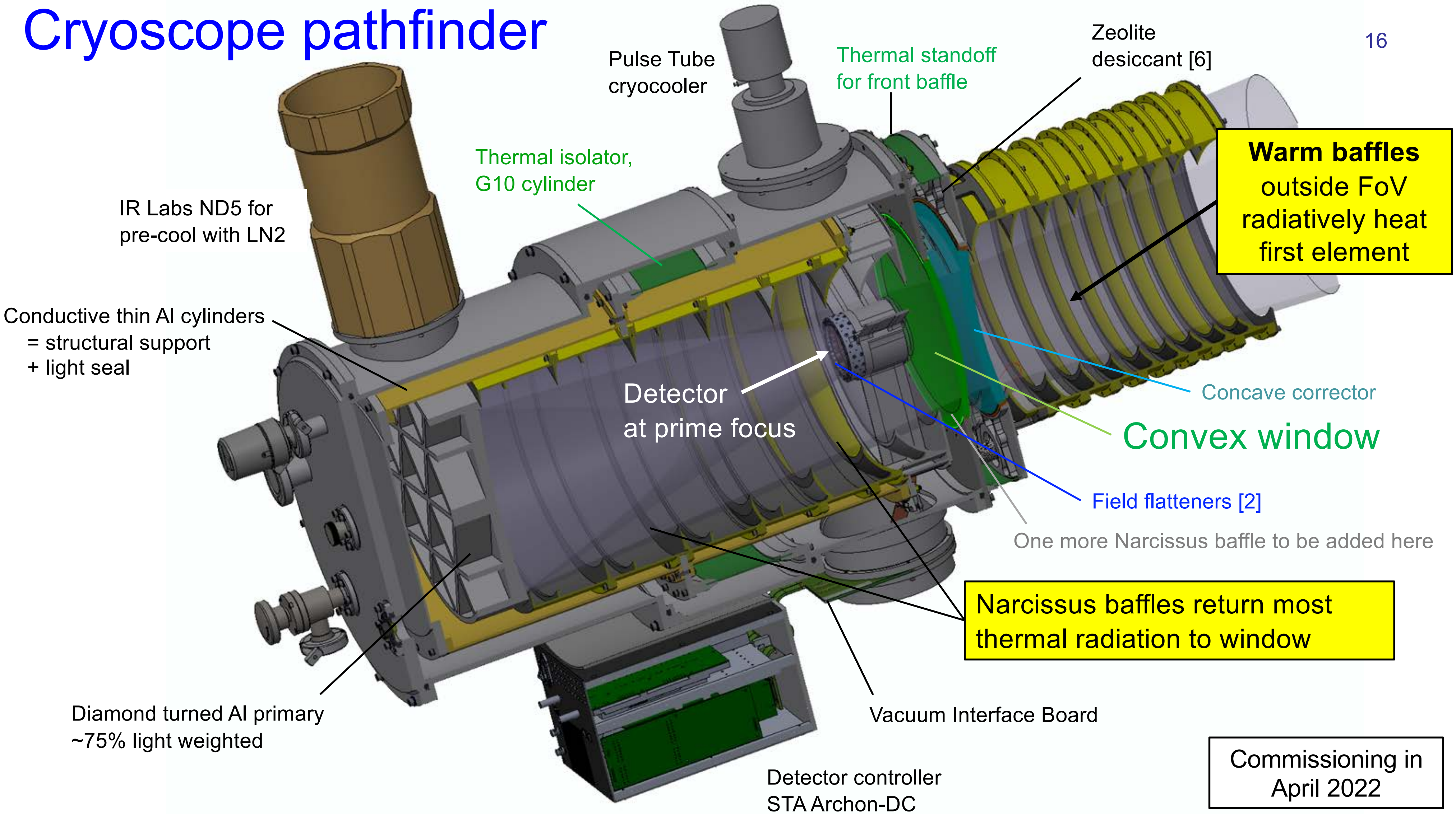

Commissioning in April 2022

Detector test system assembled

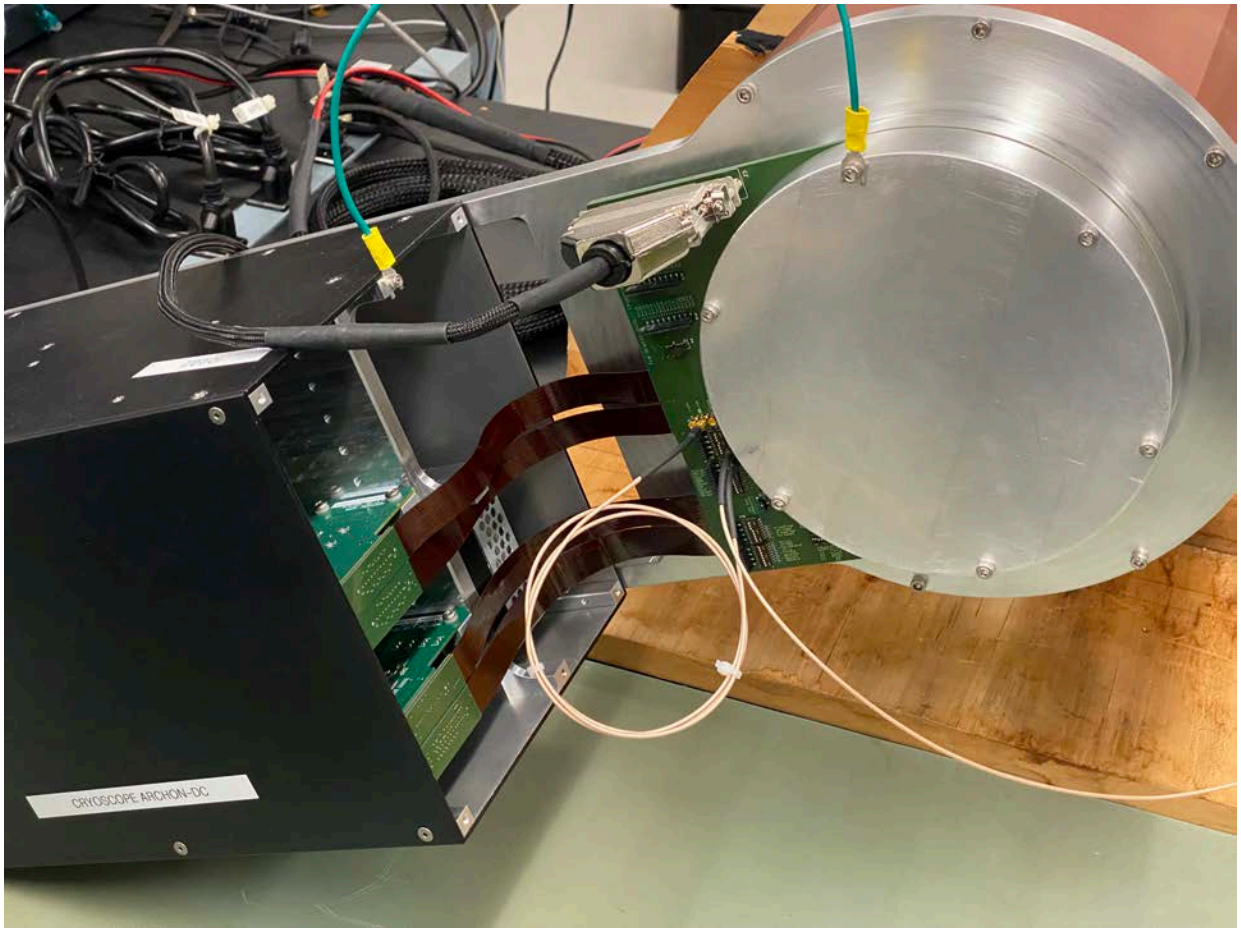

- This is a lab test dewar, not Cryoscope.
- Allows early testing of components to be used in Cryoscope: controller, wiring and detector.
- Readout waveforms in development now.
- Tests Cryoscope detector control software.

Vacuum Interface board

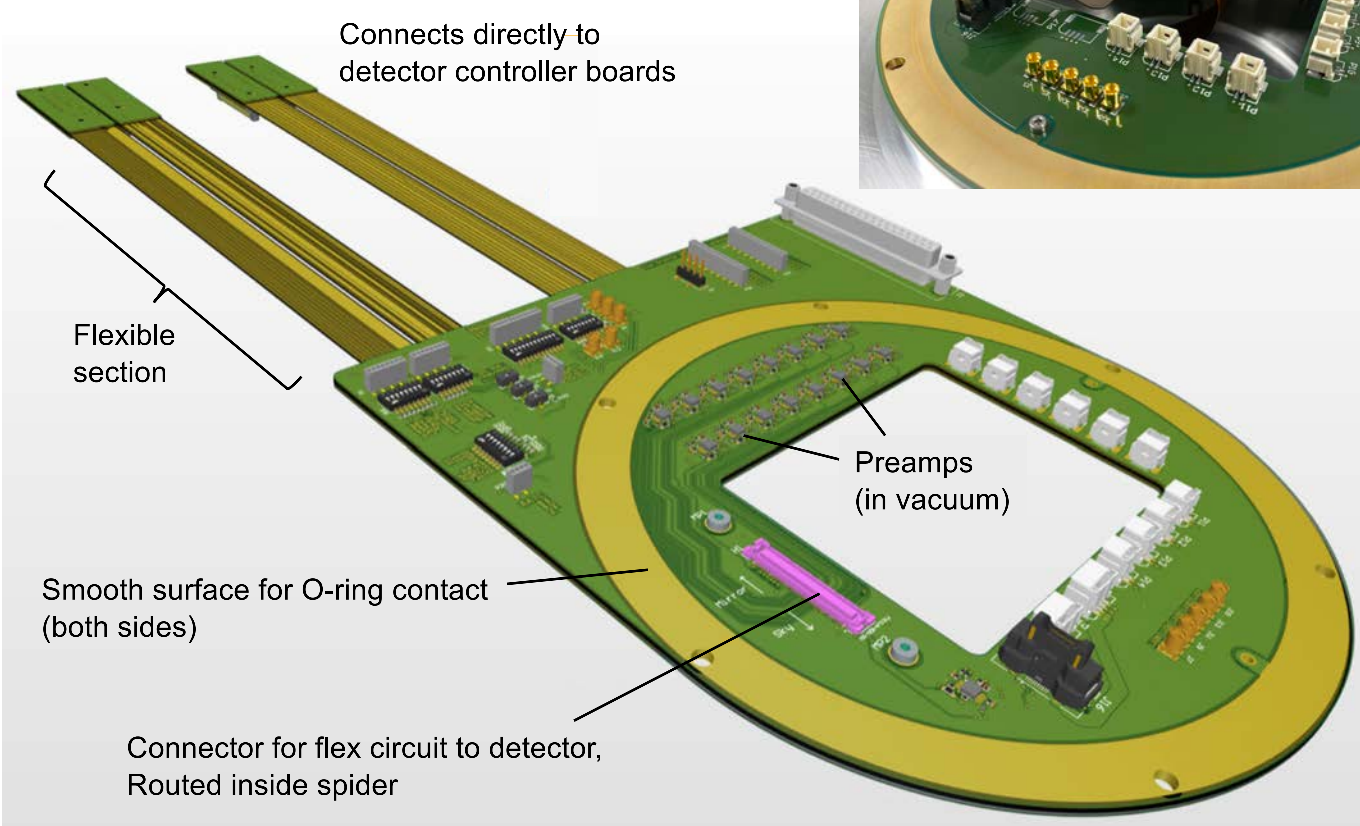

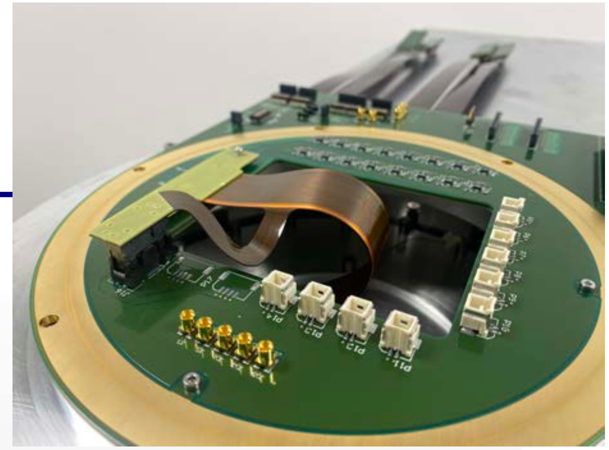

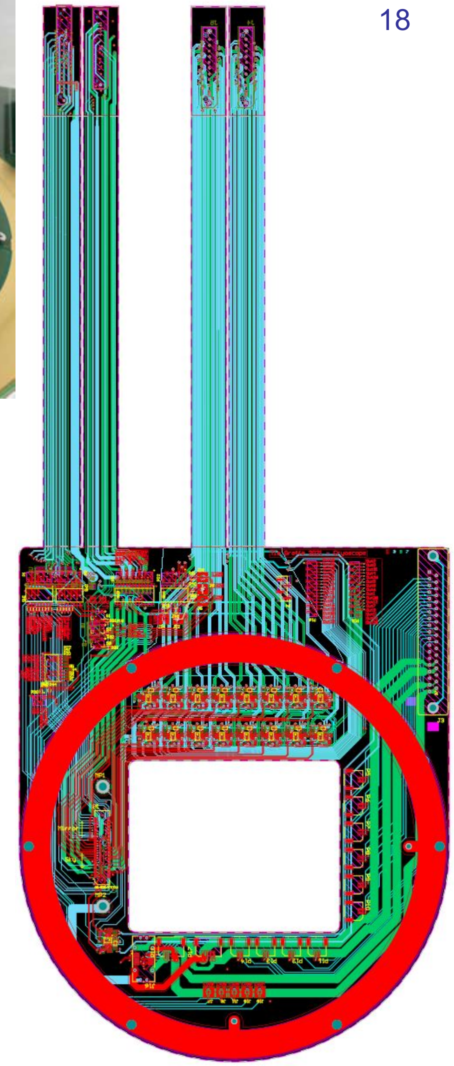

Window Stress Analysis

Tangential support by silicone gasket keeps glass in compression

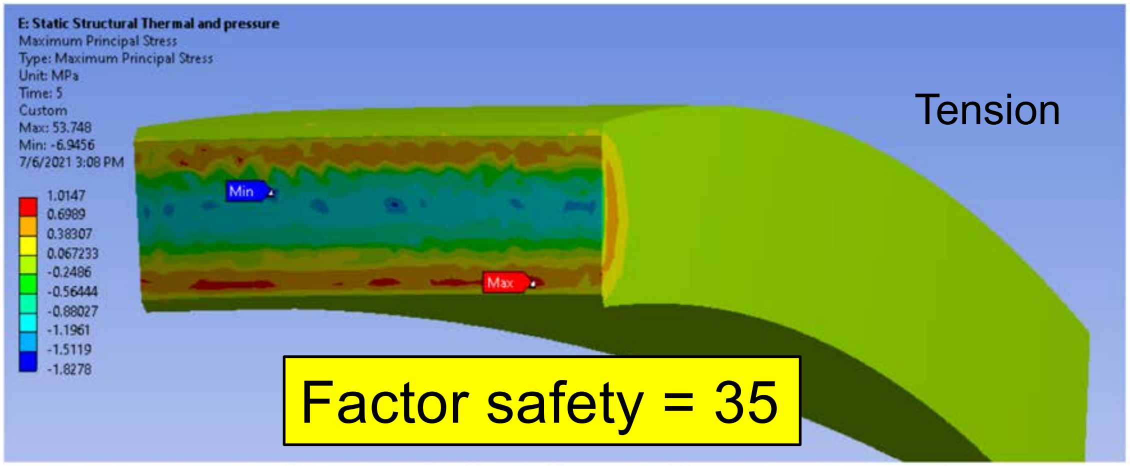

Figure 36: 8.7mm tall x 1mm thick Gasket Window Max Principal stresses at -75C

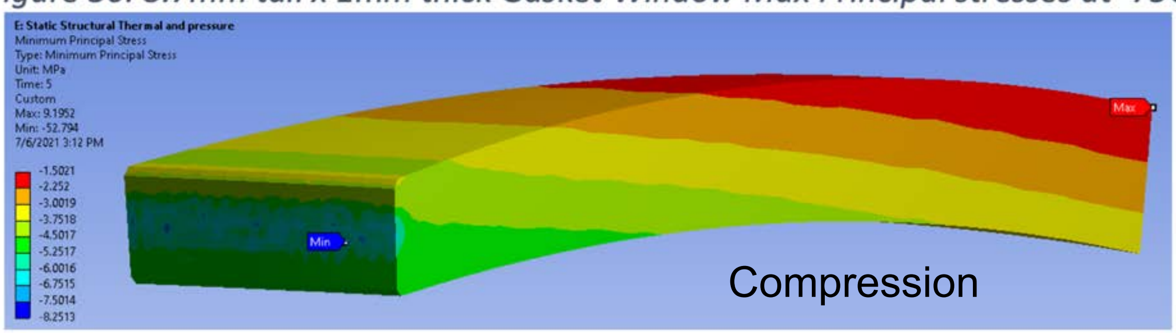

Figure 37: 8.7mm tall x 1mm thick Gasket Window Minimum Principal Stress at -75C

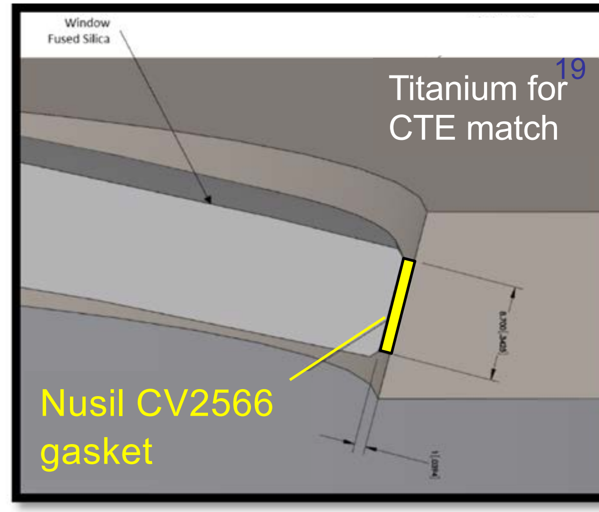

Figure 35: 8.7mm tall x 1mm thick Gasket centered on the window edg

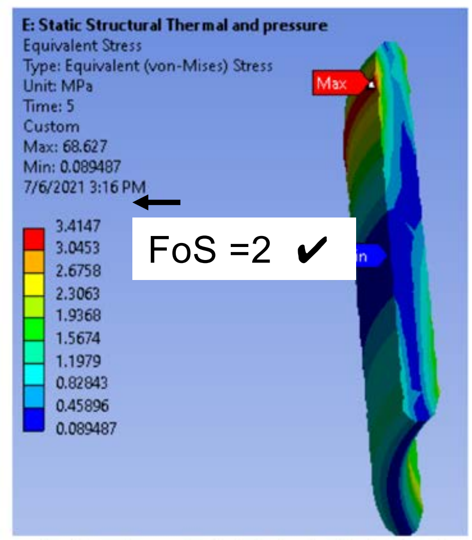

8.7mm tall x 1mm thick Gasket Equivalent Stress at -75C

>80% of radiation from window is returned to window (non-sequential ray tracing)

Config	Total Input	Total Missed*	Total Enters Window	Total Detector**	Total Exiting Window and Reflected Off Baffles**	Baffle 1**	Baffle 2**	Baffle 3**	Baffle 4**	Baffle 5**	Baffle 6**
Cone Baffles	1.0000 W	-- W	0.3990 W (100%)	0.0009 W (0.2%)	0.1758 W (44.1%)	0.1276 W (32.0%)	0.0246 W (6.2%)	0.0132 W (3.3%)	0.0072 W (1.8%)	0.0020 W (0.5%)	0.0013 W (0.3%)
Elliptical Baffles	1.0000 W	-- W	0.3990 W (100%)	0.0005 W (0.1%)	0.1990 W (49.9%)	--	--	--	--	--	--
Mixed Baffles E(2,3,4);C(1,5,6)	1.0000 W	-- W	0.3990 W (100%)	0.0005 W (0.1%)	0.1569 W (39.3%)	0.1270 W (31.8%)		0.0267 W (6.7%)		0.0020 W (0.5%)	0.0012 W (0.3%)

Since making the above table, this number has been raised to 80% with addition of baffle here

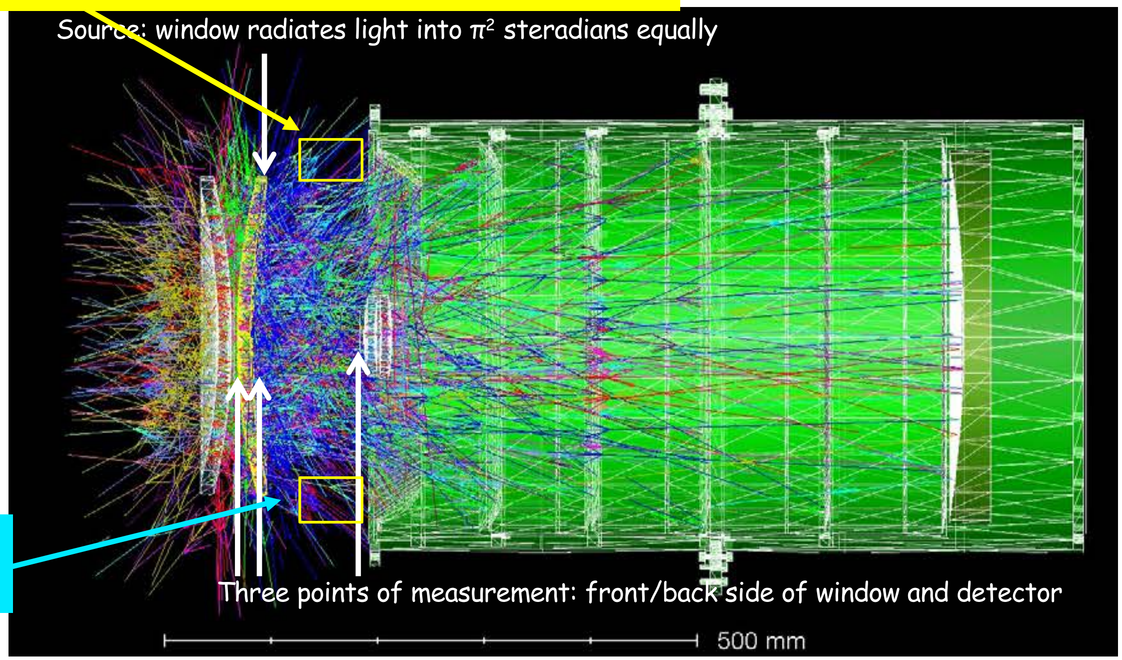

Further improvement is anticipated by filling this gap

Neglible out-of-field light scatters onto detector (non-sequential ray tracing)

Config	Total Input	Total Missed*	Total Enters Window	Total Detector**	Total Exiting Window and Reflected Off Baffles**	Baffle 1**	Baffle 2**	Baffle 3**	Baffle 4**	Baffle 5**	Baffle 6**
Cone Baffles	1.0000 W	0.3076 W	0.4499 W (100%)	0.0363 W (8.1%)	0.2361 W (52.5%)	0.0099 W (2.2%)	0.0170 W (3.8%)	0.0284W (6.3%)	0.0487 W (10.8%)	0.0710 W (15.8%)	0.0584 W (13.0%)
Elliptical Baffles	1.0000 W	0.3076 W	0.4499 W (100%)	0.0017 W (0.4%)	0.4024 W (89.4%)	--	--	--	--	--	--
Mixed Baffles E(2,3,4);C(1,5,6)	1.0000 W	0.3076 W	0.4499 W (100%)	0.0017 W (0.4%)	0.3764 W (83.7%)	0.0086 W (1.9%)		--		0.0749 W (16.6%)	0.0565 W (12.6%)

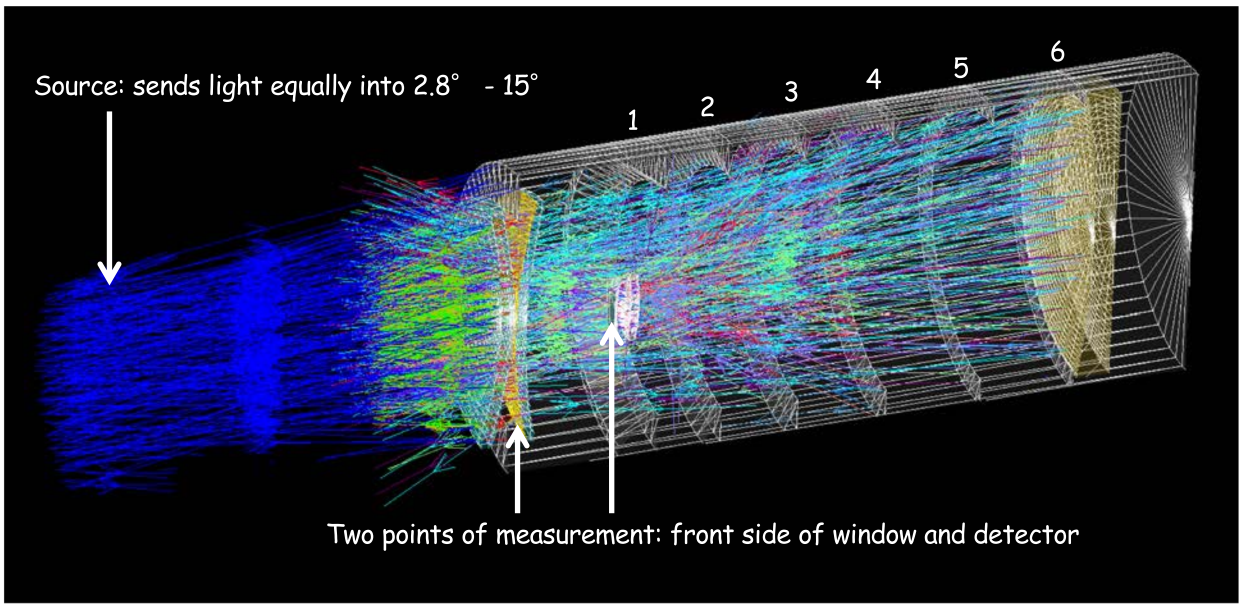

*Light that does not enter corrector lens 1.
** Percent calculated from total flux entering the window.

Flux Entering Window

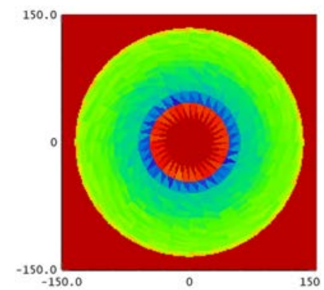

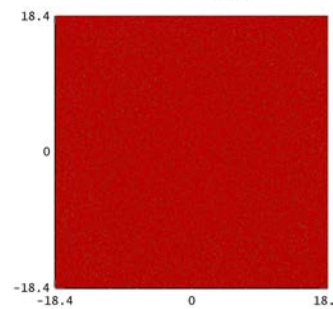

Detector Flux

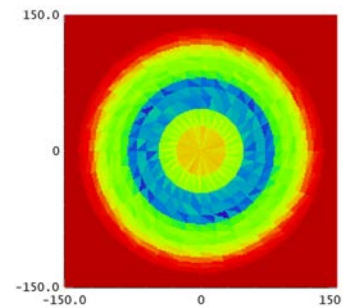

Flux Exiting Window

Dry air supply

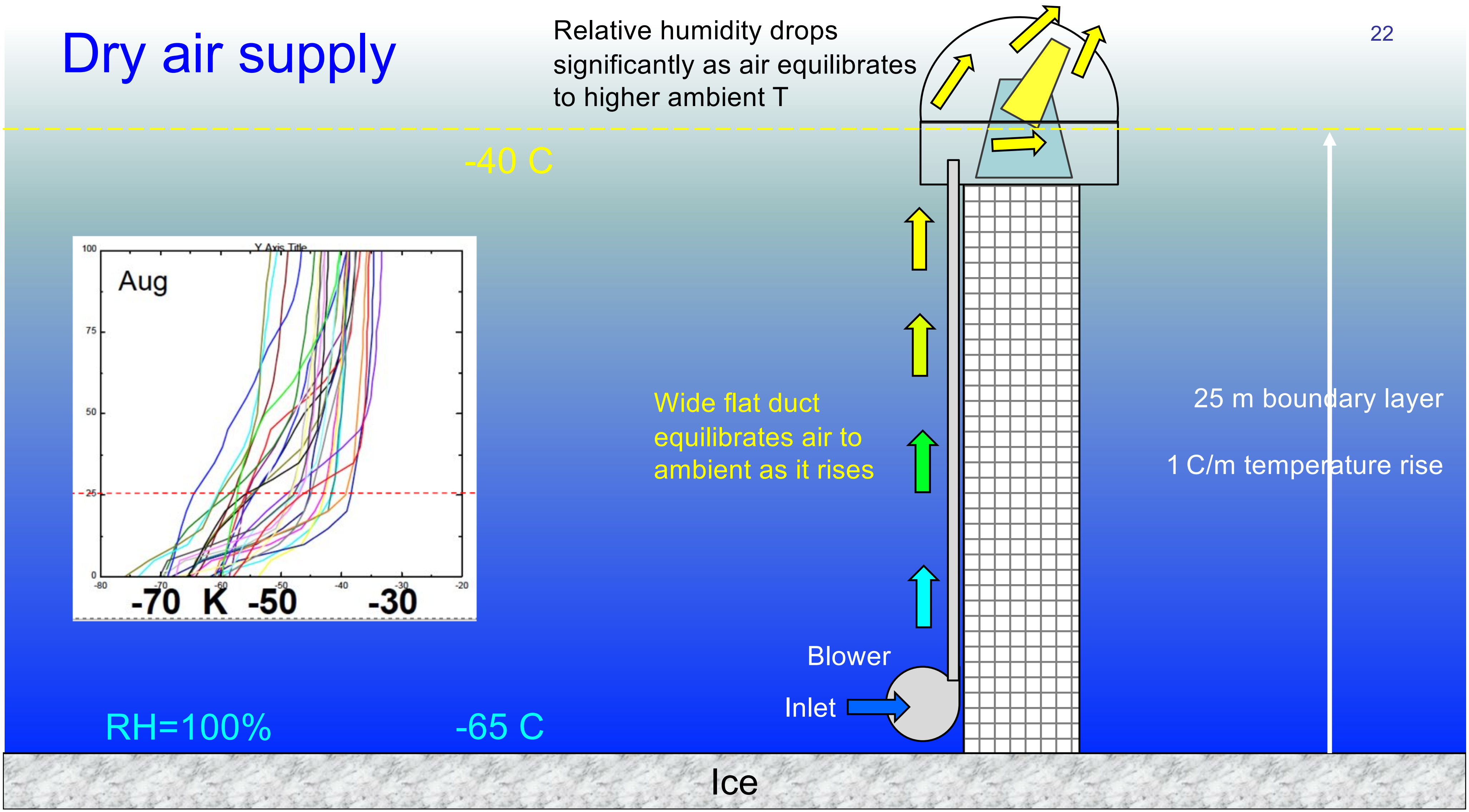

Image stabilizing telescope mount

Must isolate telescope from vibration of tower:

- Use low friction bearings rated for low temperature.
- Direct drive torque motors, so coupling is magnetic only.
- Active feedback from bright stars provided by sensor using sub-array readout.
- Use optical encoders only during slews.

Torque motor in telescope mounts by planewave.com

Custom bearings and servo are under discussion with Planewave.

Masters Student in Robotics at JHU is planning to test cryogenic bearing and develop image stabilizing servo

Conclusion

Cryoscope will validate:

- ✓ New optical design (diffraction limited over wide field)
- ✓ Cryogenic optical path
- ✓ Low sky background (when telescope emission is suppressed).
- ✓ Window temperature control (narcissus baffle performance)

✔ Good well capacity ✔ Low Interpixel Crosstalk

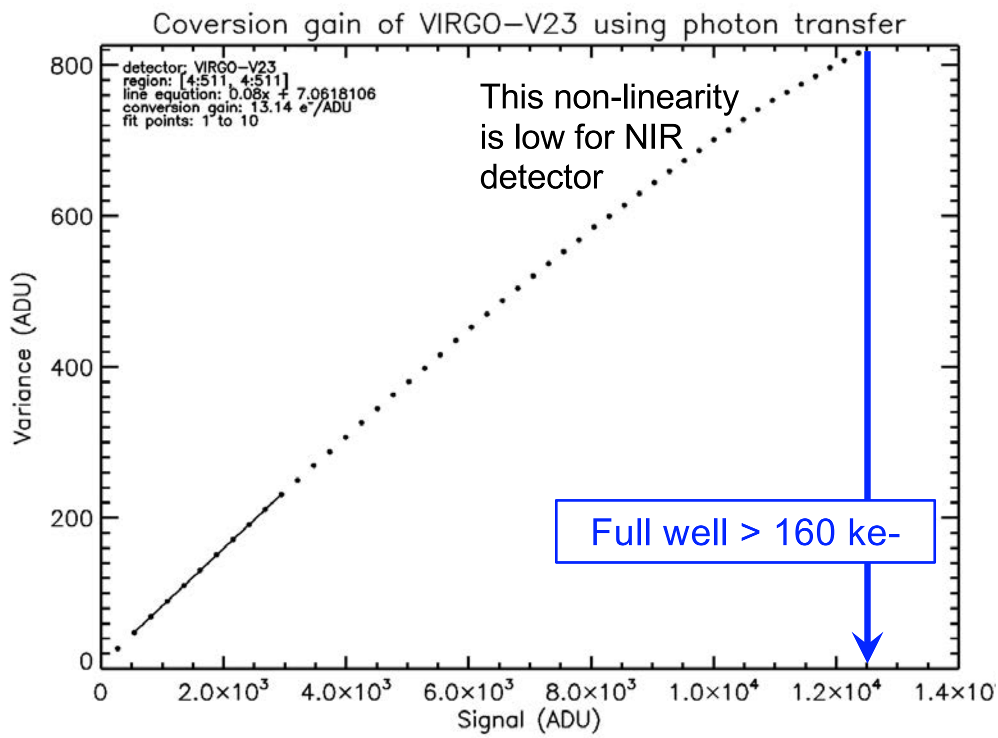

\\falcon\disk1\VIRGO−V23\cold1\JMCE\photon_xfer\photon_xfer.20Aug21\results\Q4\photon_transfer.jpg

detector temperature (K): 72.0
number of images: 10
number of events: 76
date: Fri Aug 20, 2021
region: [4:1019,4:1019]
crosstalk results (%):

−0.11	0.27	0.03
0.30	100.00	0.42
−0.04	0.31	−0.03

%

\\falcon\disk1\VIRGO−V23\cold1\JMCE\darkcurrent\darkcurrent.20Aug21_1\results\crosstalk\crosstalk_results_72.0K.jpg

Background: sky + telescope

- Low sky temperature pushes rising edge of blackbody curve beyond 2.55 μm.

- Reduced emission from telescope helps but very widefield designs have higher emissivity thus need to be colder.

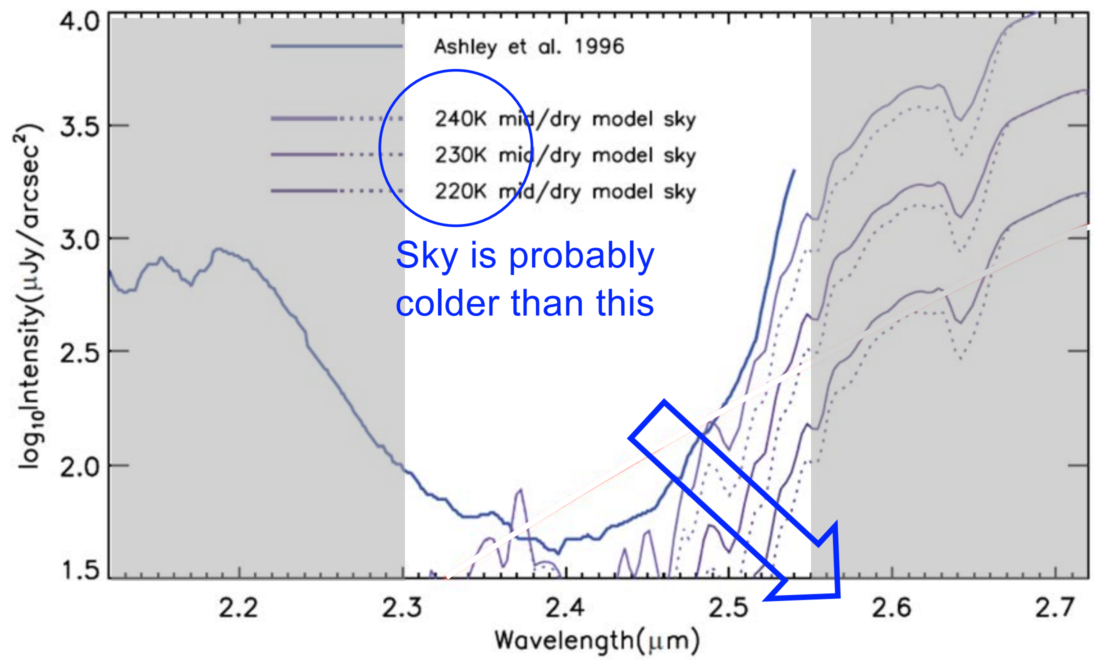

We will eliminate this

Figure 6. Measured infrared sky brightness from the South Pole taken from Ashley et al. (1996). Thermal self-emission from the instrumentation, as well as simple emissivity models assuming a cold, dry dome-A atmosphere are also presented (further details in the text). Note that Figure 1 of Phillips et al. (1999) provides additional observations of the sky from the South Pole, however these data appear to have an error in their wavelength calibration, and so are not used here.

Dome C seeing

- These numbers are for 30m above ice.
- 75% of time, seeing is better than Cryoscope diffraction limit (0.4”).

- Full potential when mounted on tower.
- Pathfinder (0.26m aperture) is small enough to be mounted on existing building.

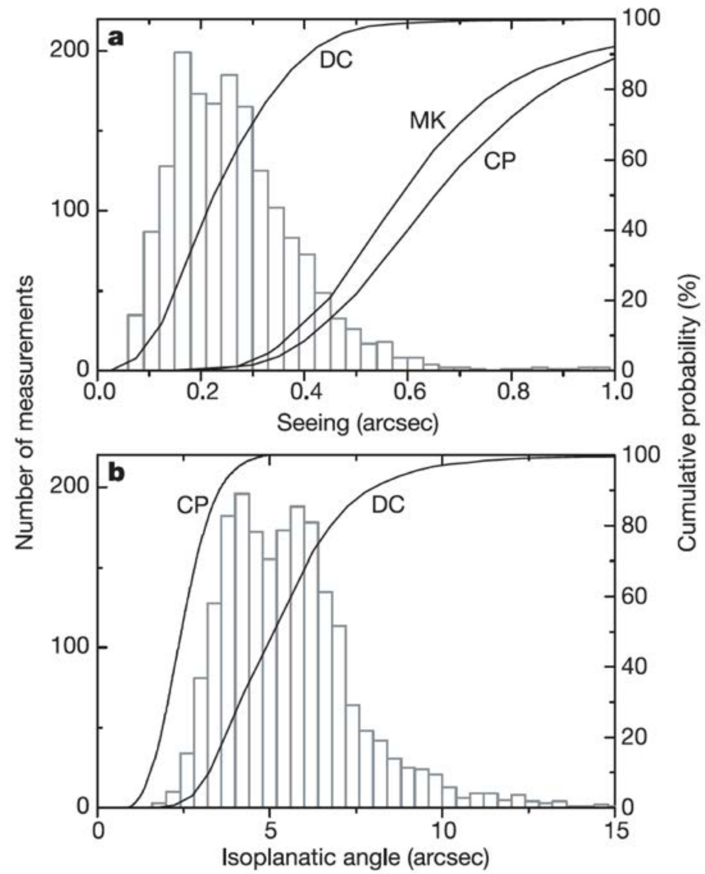

Figure 3 Histograms and cumulative distributions of the atmospheric seeing and the isoplanatic angle. **a**, Histogram of Dome C seeing above 30 m from MASS combined with SODAR, and cumulative distributions of seeing at Dome C (DC), Mauna Kea (MK) (derived from ref. 4), and Cerro Paranal (CP)[2]. **b**, Histogram of Dome C isoplanatic angle derived from the MASS instrument, and the cumulative distribution of isoplanatic angle from Dome C and Cerro Paranal[2].

Optical tolerances are quite loose

Surface Specifications → Manufacturing tolerances

Parameter	Value [mm]	Tolerance	Change to RMS WFE [nm]
L1 Center Thickness (CT)	12.5	±0.10 mm	0.00
(L1:S1) Radius of Curvature (RoC)	600.0 CC	±0.1%	2.34
(L1:S2) Radius of Curvature (RoC)	670.5 CX	±0.1%	1.52
(L1:S1) Surface Figure Errors (SFE)	0.00	<75 nm rms	0.38
(L1:S2) Surface Figure Errors (SFE)	0.00	<75 nm rms	0.44
L1 Wedge Angle	0.00	±0.017° (±1')	9.81
(L1:S2) Aspheric Surface Decenter	0.00	±0.05 mm	0.76
(L1:S1) Surface Roughness	0.00	<2.5 nm rms	na
(L1:S2) Surface Roughness	0.00	<2.5 nm rms	na
L2 Center Thickness (CT)	12.5	±0.10 mm	0.00
(L2:S1) Radius of Curvature (RoC)	600.0 CX	±0.1%	0.00
(L2:S2) Radius of Curvature (RoC)	670.5 CC	±0.1%	0.00
(L2:S1) Surface Figure Errors (SFE)	0.00	<75 nm rms	0.44
(L2:S2) Surface Figure Errors (SFE)	0.00	<75 nm rms	0.38
L2 Wedge Angle	0.00	±0.017° (±1')	13.35
(L2:S2) Aspheric Surface Decenter	0.00	±0.05 mm	1.39
(L2:S1) Surface Roughness	0.00	<2.5 nm rms	na
(L2:S2) Surface Roughness	0.00	<2.5 nm rms	na
M1 Radius of Curvature (RoC)		±0.1%	
M1 Surface Figure Errors (SFE)		<75 nm rms	
M1 Surface Roughness	0.00	<2.5 nm rms	na
L3 Center Thickness (CT)	10.0	±0.10 mm	0.26
(L3:S1) Radius of Curvature (RoC)	237.3 CX	±0.1%	0.06
(L3:S2) Radius of Curvature (RoC)	595.0 CC	±0.1%	0.00
(L3:S1) Surface Figure Errors (SFE)	0.00	<75 nm rms	0.13
(L3:S2) Surface Figure Errors (SFE)	0.00	<75 nm rms	0.06
L3 Wedge Angle	0.00	±0.017° (±1')	1.71
(L3:S2) Aspheric Surface Decenter	0.00	±0.05 mm	0.63
(L3:S1) Surface Roughness	0.00	<2.5 nm rms	na
(L3:S2) Surface Roughness	0.00	<2.5 nm rms	na
L4 Center Thickness (CT)	10.0	±0.10 mm	1.71
(L4:S1) Radius of Curvature (RoC)	241.7 CC	±0.1%	0.06
(L4:S2) Radius of Curvature (RoC)	187.7 CX	±0.1%	0.06
(L4:S1) Surface Figure Errors (SFE)	0.00	<75 nm rms	0.00
(L4:S2) Surface Figure Errors (SFE)	0.00	<75 nm rms	0.00
L4 Wedge Angle	0.00	±0.017° (±1')	0.76
(L4:S2) Aspheric Surface Decenter	0.00	±0.05 mm	0.38
(L4:S1) Surface Roughness	0.00	<2.5 nm rms	na
(L4:S2) Surface Roughness	0.00	<2.5 nm rms	na

Element Specifications → Mounting, alignment and flexure tolerances

Parameter	Value [mm]	Tolerance	Change to RMS WFE [nm]
L1 Piston (Z)	0.00	±0.200 mm	0.01
L1 Decenter (X,Y)	0.00	±0.200 mm	2.09
L1 Tilt (TX, TY)	0.00	±0.150°	8.80
L2 Piston (Z)	0.00	±0.200 mm	na
L2 Decenter (X,Y)	0.00	±0.200 mm	0.78
L2 Tilt (TX, TY)	0.00	±0.150°	13.92
M1 Piston (Z)	***na***	***±0.100 mm***	***na***
M1 Decenter (X,Y)	0.00	±0.200 mm	0.00
M1 Tilt (TX, TY)	***na***	***±0.100°***	***na***
L3 Piston (Z)	0.00	±0.200 mm	na
L3 Decenter (X,Y)	0.00	±0.200 mm	3.16
L3 Tilt (TX, TY)	0.00	±0.150°	12.91
L4 Piston (Z)	0.00	±0.200 mm	1.14
L4 Decenter (X,Y)	0.00	±0.200 mm	0.09
L4 Tilt (TX, TY)	0.00	±0.150°	3.65
Detector (Z)	0.00	±0.200 mm	1.46
Detector (X,Y)	*na*	±0.180 mm	*na*
Detector (TX,TY)	0.00	±0.02°	3.23
TOTAL RMS WFE			
EXPECTED STREHL RATIO (>80%)			
DESIGN RMS WFE	3.94		

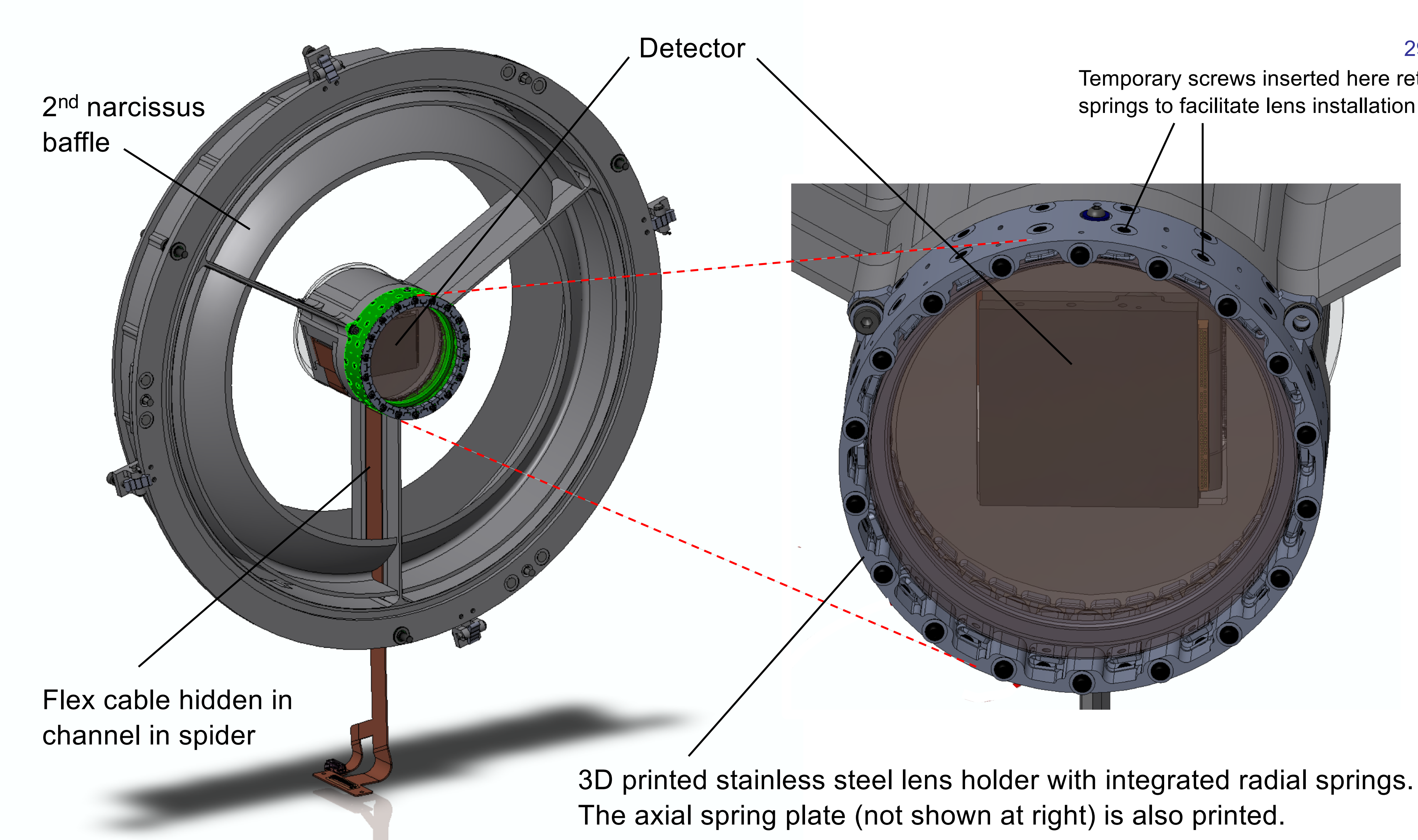
2nd narcissus baffle
Detector
Temporary screws inserted here retract springs to facilitate lens installation
Flex cable hidden in channel in spider
3D printed stainless steel lens holder with integrated radial springs.
The axial spring plate (not shown at right) is also printed.